© Copyright 2007
American Chemical Society

Langmuir
The ACS Journal of Surfaces and Colloids

MAY 22, 2007
VOLUME 23, NUMBER 11

Letters

Facile Chemical Approach to ZnO Submicrometer Particles with Controllable Morphologies

Rizia Bardhan,[†,||] Hui Wang,[†,||] Felicia Tam,[‡,||] and Naomi J. Halas*[,†,§,||]

Department of Chemistry, Department of Physics, Department of Electrical and Computer Engineering, and Laboratory for Nanophotonics, Rice University, Houston, Texas 77005

Received January 17, 2007. In Final Form: March 6, 2007

We have developed a simple wet-chemistry approach to fabricating ZnO submicrometer particles with unique morphologies including rings, bowls, hemispheres, and disks. The size and morphology of the particles can be conveniently tailored by varying the concentrations of the zinc precursor. The reaction temperature, pH, and concentration of ammonia are also found to play critical roles in directing the formation of these particle morphologies. These submicrometer particles exhibit strong white-light emission upon UV excitation as a result of the presence of surface defect states resulting from the fabrication method and synthesis conditions.

Introduction

ZnO is currently one of the most attractive semiconducting materials for optical and electronic applications because of its direct wide band gap (3.37 eV) and high exciton binding energy (60 meV).[1,2] ZnO particles have been investigated extensively as active media for applications such as luminescent light emitters,[3] solar cells,[4] phosphors,[5] and photocatalysts.[2] A proliferation of ZnO nanostructure morphologies have been reported, such as nanobelts,[3,6] nanowires,[7,8] nanorods,[9] nanotubes,[10] nanohelices,[11] tetrapods,[6,12,13] nanosheets,[14] and nanorings.[11,15] The properties of ZnO particles are highly dependent upon particle size, shape, and surface characteristics. Several fabrication techniques have been developed to prepare ZnO structures with well-defined shapes, such as vapor-phase evaporation,[7,8,16] metal−organic vapor-phase epitaxy,[17] template-based synthesis,[18] and laser ablation.[19] These fabrication pro-

* Corresponding author. E-mail: halas@rice.edu. Phone: (713) 348-5611. Fax: (713) 348-5686.
[†] Department of Chemistry.
[‡] Department of Physics.
[§] Department of Electrical and Computer Engineering.
[||] Laboratory for Nanophotonics.

(1) Djurišić, A. B.; Leung, Y. H. *Small* **2006**, *2*, 944−961.
(2) Özgür, Ü.; Alivov, Y. I.; Liu, C.; Teke, A.; Reshchikov, M. A.; Doğan, S.; Avrutin, V.; Cho, S. J.; Morkoç, H. *J. Appl. Phys.* **2005**, *98*, 041301−041404.
(3) Pan, Z. W.; Dai, Z. R.; Wang, Z. L. *Science* **2001**, *291*, 1947−1949.
(4) Kashyout, A. B.; Soliman, M.; El Gamal, M.; Fathy, M. *Mater. Chem. Phys.* **2005**, *90*, 230−233.
(5) Lin, C. H.; Chiou, B. S.; Chang, C. H.; Lin, J. D. *Mater. Chem. Phys.* **2003**, *77*, 647−654.
(6) Yan, H.; He, R.; Pham, J.; Yang, P. *Adv. Mater.* **2003**, *15*, 402−405.
(7) Huang, M. H.; Mao, S.; Feick, H.; Yan, H.; Wu, Y.; Kind, H.; Weber, E.; Russo, R.; Yang, P. *Science* **2001**, *292*, 1897−1899.
(8) Huang, M. H.; Wu, Y.; Feick, H.; Tran, N.; Weber, E.; Yang, P. *Adv. Mater.* **2001**, *13*, 113−116.
(9) Gao, P. X.; Ding, Y.; Wang, Z. L. *Nano Lett.* **2003**, *3*, 1315−1320.
(10) Kong, X. Y.; Ding, Y.; Wang, Z. L. *J. Phys. Chem. B* **2004**, *108*, 570−574.
(11) Kong, X. Y.; Wang, Z. L. *Nano Lett.* **2003**, *3*, 1625−1631.
(12) Dai, Y.; Zhang, Y.; Wang, Z. L. *Solid State Commun.* **2003**, *126*, 629−633.
(13) Roy, V. A. L.; Djurišić, A. B.; Chan, W. K.; Gao, J.; Lui, H. F.; Surya, C. *Appl. Phys. Lett.* **2003**, *83*, 141−143.
(14) Park, J. H.; Choi, H. J.; Choi, Y. J.; Sohn, S. H.; Park, J. G. *J. Mater. Chem.* **2004**, *14*, 35−36.
(15) Wang, Z. L.; Kong, X. Y.; Ding, Y.; Gao, P.; Hughes, W. L.; Yang, R.; Zhang, Y. *Adv. Funct. Mater.* **2004**, *14*, 943−956.
(16) Kong, Y. C.; Yu, D. P.; Zhang, B.; Fang, W.; Feng, S. Q. *Appl. Phys. Lett.* **2001**, *78*, 407−409.
(17) Park, W. I.; Jun, Y. H.; Jung, S. W.; Yi, G. C. *Appl. Phys. Lett.* **2003**, *82*, 964−966.
(18) Liu, C. H.; Zapien, J. A.; Yao, Y.; Meng, X.; Lee, C. S.; Fan, S.; Lifshitz, Y.; Lee, S. T. *Adv. Mater.* **2003**, *15*, 838−841.
(19) Hartanto, A. B.; Ning, X.; Nakata, Y.; Okada, T. *Appl. Phys. A* **2003**, *78*, 299.

10.1021/la070146c CCC: $37.00 © 2007 American Chemical Society
Published on Web 04/21/2007

cedures often require high-temperature conditions, prolonged reaction times, and specifically designed reactors. The development of wet-chemistry approaches to ZnO particles with controllable sizes and shapes is ultimately more desirable in terms of simplicity, efficiency, and low cost.[20−23]

ZnO is a useful and practical gain medium for solid-state UV lasers as a result of its high-quantum-efficiency photoluminescence in the UV spectral region. ZnO particles have attracted recent attention as some of the smallest lasers yet reported.[6,7,24] Meanwhile certain defects and impurities present in ZnO can also give rise to sub-band-gap states with strongly radiative decay channels. The broadband visible-light emission reported in such systems has been correlated with specific dopants and defect morphologies.[1,25−28] The sub-band-gap emission in ZnO-based materials has long been viewed as an adverse property that can be reduced by various approaches, such as annealing or placing metallic films directly adjacent to the ZnO in various device structures.[29,30] However, it has been recently realized that this visible-light emission may be a potentially valuable property, rendering ZnO a promising prospective material for solid-state lighting applications.[31]

Here we describe a simple bottom-up approach to the selective fabrication of a series of ZnO particles with unique morphologies including rings, bowls, hemispheres, and disks of various aspect ratios. The size and morphology of the particles are systematically controlled by judiciously adjusting the concentration of the precursor, zinc acetate dihydrate, in the presence of NH_4OH. The pH of the reaction mixture is also found to be critical in the formation of these well-defined shapes. The as-fabricated ZnO particles exhibit very strong broadband visible-light emission upon UV excitation, far stronger than the interband emission.

Experimental Section

Materials. Zinc acetate dihydrate ($Zn(CH_3CO_2)_2{\cdot}2H_2O$) was purchased from Sigma-Aldrich (St. Louis, MO). Ammonium hydroxide (NH_4OH, 28.8%) and 200 proof ethanol were obtained from Fisher Scientific (Hampton, NH). All chemicals were used as received without further purification. Ultrapure water (18.2 MΩ resistivity) was obtained from a Milli-Q water purification system (Millipore, Billerica, MA).

Synthesis. ZnO rings were fabricated by heating 50 mL of 200 proof ethanol in a round-bottomed flask connected to a condenser at 60 °C. While maintaining a constant temperature, 0.005 M $Zn(CH_3CO_2)_2{\cdot}2H_2O$ was introduced into the round-bottomed flask under vigorous stirring and was allowed to dissolve in the ethanol. An appropriate amount of NH_4OH (2.8 wt %, pH ∼8.2) was then added, and the reaction was continued for 45 min under vigorous stirring. After the completion of the reaction, the solution was cooled to room temperature. The resulting precipitate was centrifuged and washed several times and finally redispersed in 15 mL of ethanol. The ZnO bowls, hemispheres, and disks were fabricated by varying $Zn(CH_3CO_2)_2{\cdot}2H_2O$ concentration to 0.01 M, 0.02 M, and 0.025 M, respectively, while keeping the other experimental conditions the same.

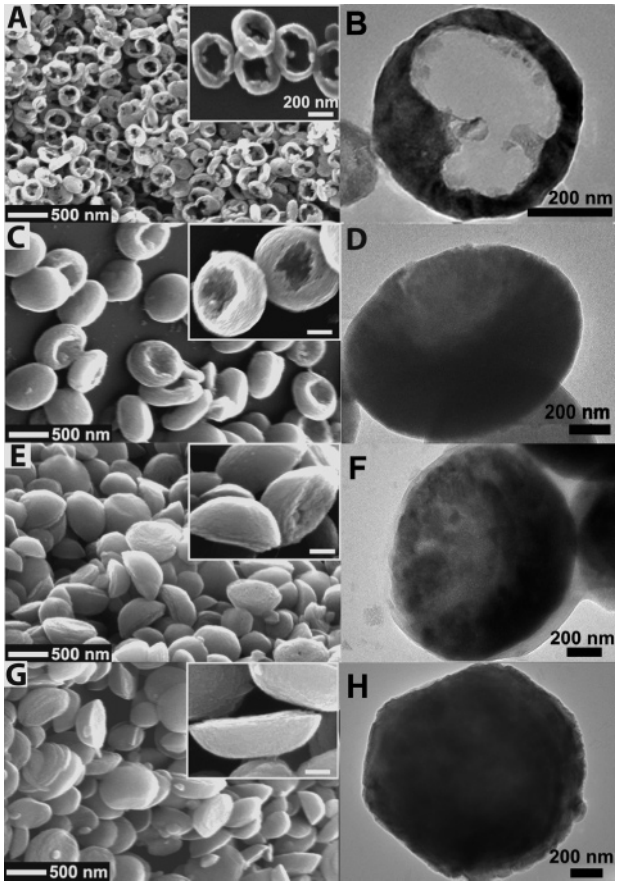

Figure 1. Low- and high-magnification (inset) SEM micrographs and corresponding TEM images of ZnO particles fabricated by varying the concentration of the Zn precursor. (A and B) Rings (0.005 M), (C and D) bowls (0.01 M), (E and F) hemispheres (0.02 M), and (G and H) disks (0.025 M). The scale bar for all of the high-magnification SEM images is 200 nm.

Characterization. Scanning electron microscope (SEM) images were obtained on a Phillips FEI XL-30 environmental SEM at an acceleration voltage of 30 kV. Transmission electron microscope (TEM) micrographs were obtained using JEOL JEM-2010 TEM. Photoluminescence (PL) spectra were obtained using a JOBIN YVON UV−vis Fluorolog, with excitation at 360 nm. All of the samples prepared for PL were maintained at the same concentration using the absorbance at 372 nm measured with a UV−vis−NIR spectrophotometer. Fluorescence images were obtained using an Axioplan-2 Imaging Zeiss fluorescence microscope with a color camera (Hg, HBO 100 W lamp, and excitation filter between 340 and 380 nm). X-ray diffraction (XRD) patterns were obtained using a Rigaku Ultima II vertical θ-θ powder diffractometer (Cu Kα, λ = 1.5418 Å).

Results and Discussion

The SEM and TEM images of the different ZnO particles fabricated by this approach are shown in Figure 1. Different morphologies can be selectively obtained by simply varying precursor concentrations within a certain pH range (Table 1). When the concentration of $Zn(CH_3CO_2)_2$ is below 0.005 M, irregular ZnO nanoparticles are obtained (Supporting Information, Figure 1S). At 0.005 M $Zn(CH_3CO_2)_2$, ZnO rings with outer diameters of 460 ± 60 nm and inner diameters of 250 ± 80 nm

(20) Liu, B.; Zeng, H. C. *J. Am. Chem. Soc.* **2003**, *125*, 4430−4431.
(21) Pal, U.; Santiago, P. *J. Phys. Chem. B* **2005**, *109*, 15317−15321.
(22) Wang, J.; Gao, L. *J. Mater. Chem.* **2003**, *13*, 2551−2554.
(23) Vayssieres, L. *Adv. Mater.* **2003**, *15*, 464−466.
(24) Yang, P.; Yan, H.; Mao, S.; Russo, R. E.; Johnson, J.; Saykally, R.; Morris, N.; Pham, J.; He, R.; Choi, H. J. *Adv. Func. Mater.* **2002**, *12*, 323−331.
(25) Wang, Y. G.; Lau, S. P.; Zhang, X. H.; Lee, H. W.; Hng, H. H.; Tay, B. K. *J. Cryst. Growth* **2003**, *252*, 265−269.
(26) Roy, V. A. L.; Djurišić, A. B.; Liu, H.; Zhang, X. X.; Leung, Y. H.; Xie, M. H.; Gao, J.; Lui, H. F.; Surya, C. *Appl. Phys. Lett.* **2004**, *84*, 756−758.
(27) Gao, S.; Zhang, H.; Deng, R.; Wang, X.; Sun, D.; Zheng, G. *Appl. Phys. Lett.* **2006**, *89*, 1231251−1231253.
(28) Foreman, J. V.; Li, J.; Peng, H.; Choi, S.; Everitt, O. H.; Liu, J. *Nano Lett.* **2006**, *6*, 1126−1130.
(29) Djurišić, A. B.; Choy, W. C. H.; Roy, V. A. L.; Leung, Y. H.; Kwong, C. Y.; Cheah, K. W.; Gundu Rao, T. K.; Chan, W. K.; Lui, H. F.; Surya, C. *Adv. Func. Mater.* **2004**, *14*, 856−864.
(30) Lin, H. Y.; Cheng, C. L.; Chou, Y. Y.; Huang, L. L.; Chen, Y. F.; Tsen, K. T. *Opt. Express* **2006**, *14*, 2372−2379.
(31) Sui, X. M.; Shao, C. L.; Liu, Y. C. *Appl. Phys. Lett.* **2005**, *87*, 1131151−1131153.

Table 1. Synthesis Parameters and Morphology of Different ZnO Structures

concentration of $Zn(Ac)_2$ (M)	pH (NH_4OH 2.8%) initial	final	morphology	size (nm)
0.001	4.4	6.4	irregular nanoparticles	
0.005	4.2	5.5	rings	460 ± 60
0.01	4.2	5.5	bowls	710 ± 80
0.002	4.0	5.5	hemispheres	790 ± 85
0.025	4.0	5.5	disks	910 ± 70
0.04	4.0	6.2	agglomerated particles	
0.05	3.9	6.2	agglomerated particles	
0.01[a]	4.3	5.6	inhomogeneous matrix	
0.02[a]	4.1	5.5	inhomogeneous matrix	

[a] We used KOH instead of NH_4OH maintained at similar pH.

are formed (Figure 1A,B). A further increase in the concentration of the Zn precursor to 0.01 M results in submicrometer bowl-shaped structures with an average size of 710 ± 80 nm and an inner diameter of 260 ± 50 nm (Figure 1C,D). The inset of Figure 1C shows striations along the radial direction, suggesting the preferential growth along the radius of the ZnO crystals to form this unusual structure. Submicrometer hemispheres are formed when the concentration of precursor is increased to 0.02 M (Figure 1E,F). These particles are 790 ± 85 nm in diameter and clearly display a smooth outer surface but coarse inner surface with visible crystalline facets. As the concentration of $Zn(CH_3CO_2)_2$ is further increased to 0.025 M, disklike shapes are formed (Figure 1G,H). Although increasing the precursor concentration from 0.02 to 0.025 M did not radically change the morphology of the particles, the hemispheres appeared to increase radially without a considerable change in depth, resulting in such a disklike shape. These disks (average size ~910 ± 70 nm) exhibit a quasihexagonal cross section (Figure 1H). At zinc acetate concentrations above 0.03 M, larger particles are formed with significant agglomeration and indefinite morphology (Supporting Information Figure 2S). Therefore, it appears that only over a limited range of Zn^{2+} concentration are the fabrication conditions appropriate for the formation of ZnO particles with these well-defined morphologies.

The crystallinity of the ZnO particles obtained at different concentrations of Zn $(CH_3CO_2)_2$ was also investigated. Figure 2A shows the XRD patterns of all of the obtained morphologies—rings, bowls, hemispheres, and disks. The XRD patterns exhibit sharp peaks, indicating that the particles possess large crystalline domains as well as a high degree of crystallinity. Figure 2B shows the TEM image of a submicrometer bowl and the corresponding electron diffraction (ED) pattern, revealing that the bowl structures are composed of several crystalline domains. Selected-area electron diffraction (SAED) (Figure 2B, bottom inset, area shown in circle) shows a single-crystalline domain with hexagonal wurtzite structure along the [0001] zone axis in this region. The TEM image and corresponding SAED patterns of a submicrometer ring are illustrated in Figure 2C. The two selected regions in the ring (areas shown in the circle) have crystalline domains with hexagonal wurtzite structure along the [0001] zone axis. However, the crystalline domians are oriented differently, verifying the polycrystallinity of the particles.

The growth mechanism and resulting crystal structure of these ZnO particles can be interpreted in the context of supersaturation, nucleation, Ostwald ripening, and oriented attachment.[32] The kinetics of crystal growth and coarsening strongly depends on the structure of the material, the surface chemistry of the particles resulting from ions in the solution, and the interface between the

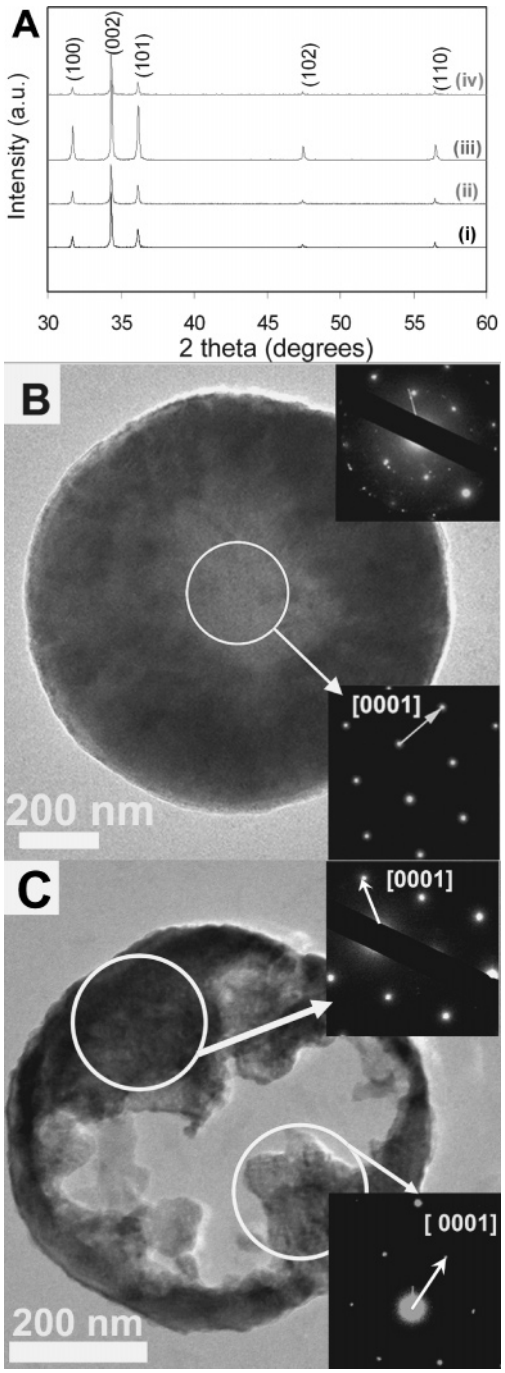

Figure 2. Crystallographic studies of the ZnO particles obtained at different concentrations of the Zn precursor. (A) XRD patterns of (i) rings (0.005 M), (ii) bowls (0.01 M), (iii) hemispheres (0.02 M), and (iv) disks (0.025 M). (B) TEM image of a submicrometer bowl with the corresponding ED pattern (top inset) and the SAED pattern (bottom inset, area shown in circle) characteristic of these structures. (C) TEM image of a polycrystalline ring. The SAED patterns (areas shown in circles) illustrate crystalline domains along different orientations.

crystals and surrounding solution.[33] At a Zn precursor concentration lower than 0.005 M, an insufficient amount of solute is present to yield a supersaturated solution. At 0.005 M Zn^{2+}, nucleation occurs since a supersaturated solution is achieved. The ZnO nuclei further grow by a diffusive mechanism forming primary particles.[32] These small crystalline primary particles subsequently aggregate through oriented attachment, forming

(32) Hu, Z.; Oskam, G.; Penn, R. L.; Pesika, N.; Searson, P. C. *J. Phys. Chem. B* **2003**, *107*, 3124−3130.

(33) Banfield, J. F.; Welch, S. A.; Zhang, H.; Ebert, T. T.; Penn, R. L. *Science* **2000**, *289*, 751−754.

Table 2. Concentration of Ammonia and Morphology of ZnO Structures

	pH of reaction		
NH_4OH wt %	initial	final	morphology
1.12	3.9	4.8	distorted bowls
2.8	4.2	5.5	bowls
5.6	4.4	6.3	inhomogeneous matrix
8.4	4.9	7	inhomogeneous matrix
11.2	5.1	7.2	inhomogeneous matrix

secondary particles.[33−35] Oriented attachment involves the self-organization of adjoining particles such that regular crystallographic orientation is achieved, followed by joining these particles at a planar interface.[35] Oriented attachment usually results in single crystals, which could explain the single-crystalline domains found in the bowls and rings (Figure 2B,C). However, the orientation adopted within one region is dissimilar to that in an adjacent region in the reaction mixture. Therefore, following the aggregation process, polycrystalline structures composed of several single-crystalline domains are obtained. In solution-phase synthesis, the formation of large polycrystalline particles with complex morphologies is not surprising. When the Zn precursor concentration is increased, Ostwald ripening controls crystal growth by the diffusion of ions along the matrix−particle boundary and results in larger particle sizes.[34] The observed differences in morphology with increasing concentration of $Zn(CH_3CO_2)_2$ could be due to the simultaneous occurrence of Ostwald ripening and oriented attachment during the growth of crystals.[34,36] Whereas Ostwald ripening leads to spherical/hemispherical shapes with a smooth edge, oriented attachment forms irregular shapes with visible facets. The smooth outer surfaces of the bowls, hemispheres, and disks with irregularly faceted inner surfaces verify this theory (Figure 1C, E, and G, respectively).

In addition to the effect of precursor concentration on the particle morphologies, the pH of the reaction mixture also influences the shape evolution of the particles (Table 1). Although the exact mechanism of formation of these unique morphologies is debatable,[37,38] we believe that besides the $Zn(CH_3CO_2)_2$ concentration the difference between the initial and final pH values of the reaction mixture may control the nucleation and growth event.[21] Larger differences between the initial and final pH values of the reaction mixture result in a higher nucleation rate; consequently, ZnO particles are formed at a rapid rate, leading to agglomerated particles with indefinite morphology. When the variation between initial and final pH values of the reaction mixture is small, the nucleation rate is slower, leading to the development of well-defined particle shapes with different sizes. The ZnO submicrometer rings, bowls, hemispheres, and disks are formed when the difference between the initial and final pH values of the reaction is ∼1.3−1.5.

We have also investigated the precise pH range within which well-defined morphologies were obtained by varying the concentration of NH_4OH (Table 2) while maintaining a constant precursor concentration of 0.01 M. Whereas distorted bowl-like shapes were observed (Supporting Information, Figure 3S) at a lower concentration of NH_4OH (1.12 wt %), an inhomogeneous matrix was obtained at a higher concentration of NH_4^+ (Supporting Information, Figures 4S and 5S). It appears that at a final pH value of ∼4.8 the reaction solution may be excessively acidic, forming distorted particles; additionally, at final pH values >6, the reaction conditions were unsuitable for forming any distinctive structure. We also observed that at a higher concentration of NH_4OH (5.6 wt % and above) the difference between the initial and final pH values of the reaction also increases, which explains the formation of matrices with no particular morphology. From these observations, it appears that in addition to the Zn precursor only a certain pH range is suitable for the formation of ZnO nuclei in solution, influencing the crystal growth rate and the resulting morphologies.

In addition to the precursor concentration and reaction pH, the effects of reaction temperature and the formation of a zinc ammonia ligand on the particle size and morphologies were also investigated to gain better insight into possible growth mechanisms. The particles reported here form only at ∼60 °C. At temperatures below 60 °C, only amorphous ZnO nanoparticles were formed. At reaction temperatures higher than 60 °C (70, 80 °C), the formation of an extended ZnO matrix was observed. It thus appears that only at temperatures near 60 °C does ZnO nucleate and aggregate into the observed morphologies. We also observed that the presence of ammonium cations was essential for the formation of the reported particles (rings, bowls, hemispheres, and disks). Wang et al.[39] have reported that NH_4^+ ions may adsorb onto the surface of ZnO crystals as a result of the high surface energy associated with the nanophase materials and thus affect crystal growth. This may also be occurring in the system reported here and may influence the shape of the particle morphologies. Alternatively, NH_4^+ may participate in the reaction by forming a zinc ammonia ligand ($Zn(NH_3)_4^{2+}$), which would then directly affect the morphology of the structures.

$$Zn^{2+} + NH_3 \rightarrow Zn(NH_3)_4^{2+} \quad (1)$$

$$Zn(NH_3)_4^{2+} + OH^- \rightarrow ZnO \quad (2)$$

We confirmed the significance of the NH_4^+ cations as a structure-directing agent by replacing NH_4OH with KOH, maintaining a pH (∼ 8.2) that is similar to that of the original ammonium hydroxide reactant solution (Table 1). In this case, none of the reported morphologies were observed; instead, large ZnO particles, which subsequently coalesced to form a matrix, were achieved (Supporting Information, Figures 6S and 7S). Certain ligands have been known to exert thermodynamic control over chemical systems and influence crystal orientation through the metal−ligand bond length, ligand strength, and energy associated with metal−ligand bond formation.[40] Therefore, we infer that in addition to zinc acetate concentration and reaction pH, the presence of NH_4^+ may also guide the structural formation of these ZnO submicrometer particles, possibly by forming the $Zn(NH_3)_4^{2+}$ ligand during the course of the reaction.

Although these particles are highly crystalline, they also possess a large concentration of surface defect states, which is directly related to the fabrication route and synthesis conditions. Optical studies of these particles reveal the presence of surface defects. The as-fabricated ZnO particles exhibit strong photoluminescence upon UV excitation. Figure 3A shows an image of white-light emission from a film of ZnO hemispheres. The rings, bowls, and disks all exhibit extremely similar light-emitting properties (Figure 3B). The PL spectra of all particles show a weak interband emission at 370−389 nm (3.19−3.35 eV) and a broad visible

(34) Huang, F.; Zhang, H.; Banfield, J. F. *Nano Lett.* **2003**, *3*, 373−378.
(35) Penn, R. L.; Banfield, J. F. *Science* **1998**, *281*, 969−971.
(36) Huang, F.; Zhang, H.; Banfield, J. F. *J. Phys. Chem. B* **2003**, *107*, 10470−10475.
(37) Li, W. J.; Shi, E. W.; Zhong, W. Z.; Yin, Z. W. *J. Crys. Growth* **1999**, *203*, 186−196.
(38) Baxter, J. B.; Wu, F.; Aydil, E. S. *Appl. Phys. Lett* **2003**, *83*, 3797−3799.
(39) Wang, L.; Muhammed, M. *J. Mater. Chem.* **1999**, *9*, 2871−2878.
(40) DiLeo, L.; Romano, D.; Schaeffer, L.; Gersten, B.; Foster, C.; Gelabert, M. C. *J. Cryst. Growth* **2004**, *271*, 65−73.

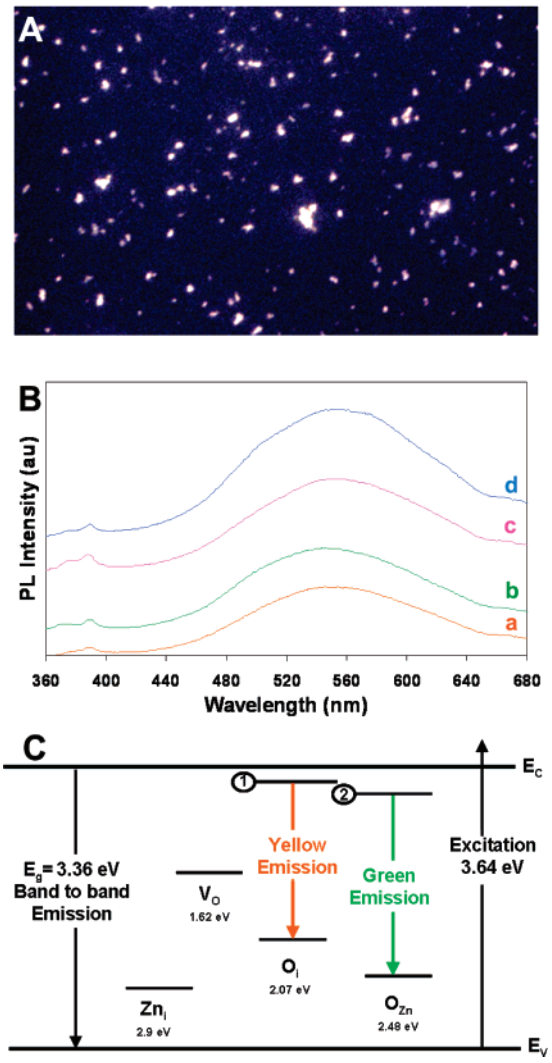

Figure 3. (A) Fluorescence image of ZnO hemispheres emitting white light upon UV excitation. (B) PL spectra of the observed ZnO particles normalized relative to particle concentration: (a) rings, (b) bowls, (c) hemispheres, and (d) disks. Weak interband emission is observed at 370−389 nm, and strong visible emission centered at ~558 nm. The spectra are offset for clarity. (C) Energy diagram of defect states in ZnO.

band centered at ~558 nm (2.22 eV). The visible band spans from ~420 to 700 nm for all ZnO particle morphologies reported here.

Various explanations have been proposed for the white-light emission from ZnO based on oxygen or zinc defect states. The broadband visible-light emission observed in these particles may be attributable to a combination of oxygen interstitial defects (O_i) and antisite oxygen defects (O_{Zn}).[1,41] Oxygen interstitial defects have been reported to be responsible for yellow emission, and antisite oxygen defects cause green emission as illustrated in the energy diagram of ZnO defect levels (Figure 3C). A photogenerated hole is trapped at the surface by interstitial oxygen defects or antisite oxygen defects; it then migrates to deeply trapped levels located above the valence band. Broad visible emission occurs when the photogenerated hole trapped in a deep level recombines with a photogenerated electron trapped in a shallow level (levels 1 and 2, respectively).[1,42] Depending on the temperature and the presence of oxygen during sample preparation, a mixture of oxygen defect states can be created, many of which can produce visible light. The precise origin of the broadband emission from these unique particles is still under investigation, yet the large ratio of the visible PL intensity to the interband PL intensity in these polycrystalline structures indicates the presence of a large number of surface defects.

Conclusions

In summary, by controlling the growth kinetics through precursor concentration, reaction temperature, pH, and the type and concentration of ions present in solution, we have fabricated ZnO submicrometer particles including rings, bowls, hemispheres, and disks of varying aspect ratio. The broad emission from the ZnO particles covering most of the visible region may be attributable to a combination of oxygen defect states resulting from the fabrication conditions. Future studies may be useful in advancing our understanding of the growth mechanism of hemispherical ZnO particles in comparison to that of rod- or ribbonlike ZnO particles. In addition, future studies of the properties of these ZnO particles may lead to the development of economical, white-light-emitting materials for solid-state lighting applications.

Acknowledgment. We gratefully acknowledge NSF (EEC-0304097), AFOSR (F49620-03-C-0068), the Robert A. Welch Foundation (C-1220), and MURI (W911NF-04-01-0203) for financial support. We thank William Deery, Peter Loos, Joseph Cole, Nathaniel Grady, and Bruce Brinson for their assistance.

Supporting Information Available: SEM images of ZnO particles with varied morphologies obtained under different conditions. This material is available free of charge via the Internet at http://pubs.acs.org.

LA070146C

(41) Greene, L. E.; Law, M.; Goldberger, J.; Kim, F.; Johnson, J. C.; Zhang, Y.; Saykally, R. J.; Yang, P. *Angew. Chem., Int. Ed.* **2003**, *42*, 3031−3034.
(42) Kahn, M. L.; Cardinal, T.; Bousquet, B.; Monge, M.; Jubera, V.; Chaudret, B. *ChemPhysChem* **2006**, *7*, 2392−2397.

Supporting Information

A Facile Chemical Approach to ZnO Submicron Particles with Controllable Morphologies

Rizia Bardhan[1,4], *Hui Wang*[1,4], *Felicia Tam*[2,4], and *Naomi J. Halas*[1,3,4,]*

[1] Department of Chemistry, [2] Department of Physics, [3] Department of Electrical and Computer Engineering, and [4] the Laboratory for Nanophotonics, Rice University, Houston, TX 77005
* Corresponding author

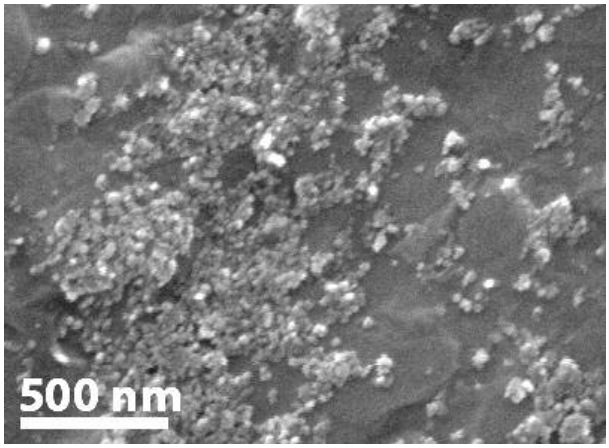

Figure 1S: Irregular ZnO nanoparticles obtained at 0.001 M of $Zn(CH_3CO_2)_2$

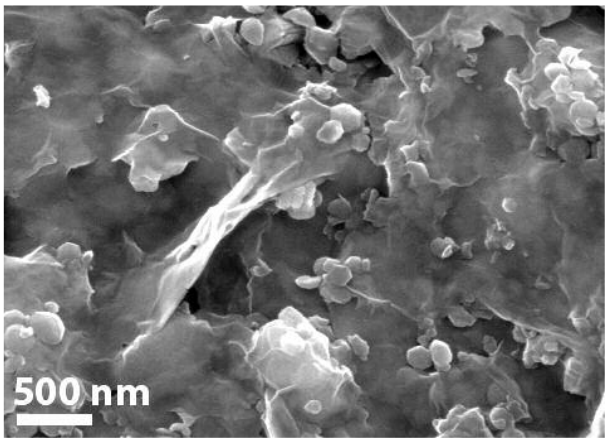

Figure 2S: Agglomerated ZnO particles obtained at 0.04M of $Zn(CH_3CO_2)_2$

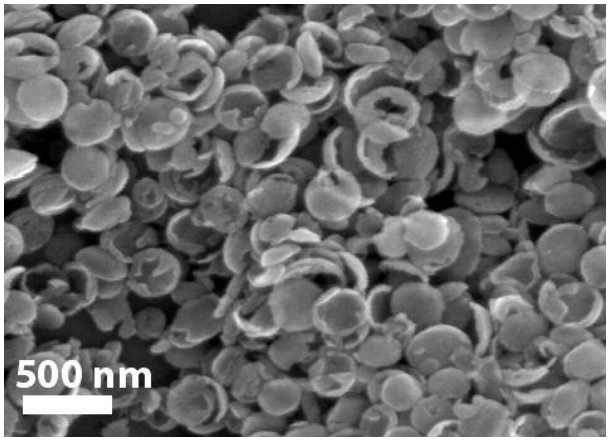

Figure 3S: Distorted bowl-like shapes obtained at lower concentration of NH_4OH (1.12 wt %)

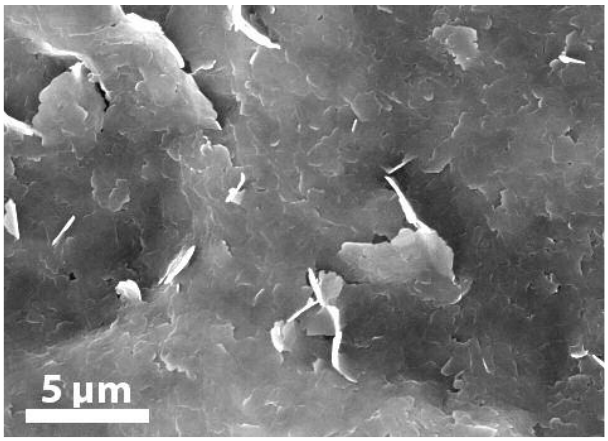

Figure 4S: Inhomogeneous matrix obtained at 5.6 wt % of NH_4OH

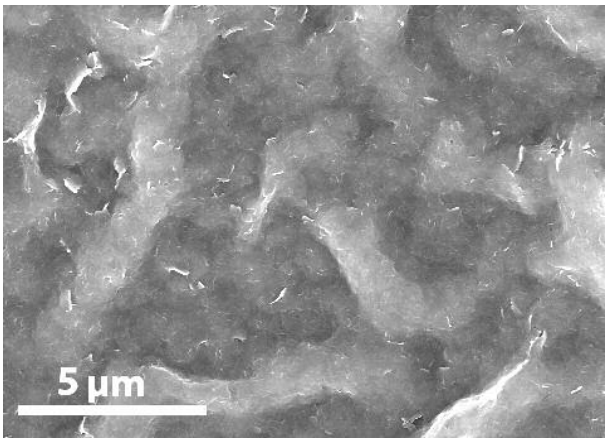

Figure 5S: Matrix obtained at higher concentration of NH_4OH (8.4 wt % and 11.2 wt %)

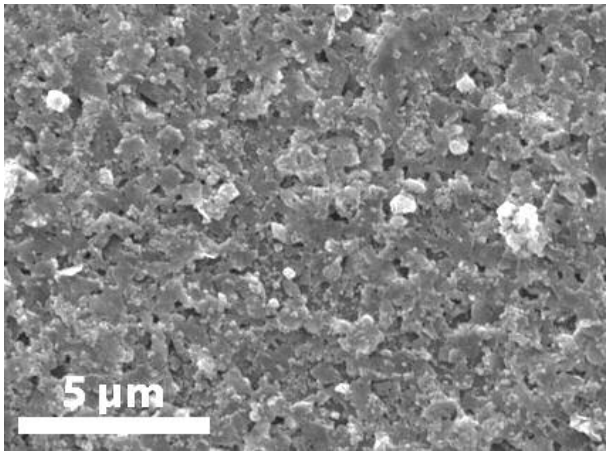

Figure 6S: ZnO matrix obtained at 0.01 M $Zn(CH_3CO_2)_2$ and KOH (pH ~ 8.2)

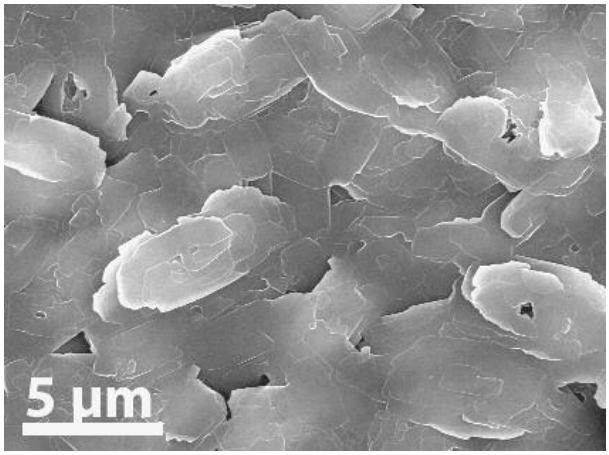

Figure 7S: ZnO inhomogeneous matrix obtained at 0.02 M of $Zn(CH_3CO_2)_2$ and KOH (pH ~ 8.2)